Conception of minichannel cooling for a PVT heat exchanger

Dariusz Strąk[1*], and *Magdalena* Piasecka[1]

[1]Kielce University of Technology, Faculty of Mechatronics and Mechanical Engineering, Al. 1000-lecia Panstwa Polskiego 7, 25-314 Kielce, Poland

Abstract. In the paper, a new construction of a compact plate heat exchanger dedicated to PVT cooling was numerically tested. The efficiency of photovoltaic panels decreases as their temperature increases, but cooling improves efficiency. A model counter-current heat exchanger with rectangular minichannels was presented. A heated wall of the heat exchanger was a photovoltaic cell. There were laminar flows of Fluorinert FC-72 and distilled water in the minichannels. FC-72 was heated by the photovoltaic panel. The CAD model of a minichannel heat exchanger was proposed. CFD calculations were performed using Simcenter STAR-CCM+ software. The fluid temperature and velocity profile in the minichannels were determined to finally obtain the values of the heat transfer coefficient. The main parameters taken into consideration in the computations concerned: meshes, physics, and geometry. Finally, local heat transfer coefficients were determined.

1 Introduction

The increased demand for energy, the limited amount of fossil resources and the excessive pollution of the environment have caused great interest in renewable energy sources in recent years. One type of renewable energy source is solar energy, which can be converted into electricity through the use of photovoltaic cells. During sunny days, photovoltaic panels can heat up to a temperature of about 50 - 60 °C. When solar panels are heated, their efficiency and service life decrease. It is estimated that as the temperature of the panels increases every 1°C, their efficiency decreases by approximately 0.5% [1]. To increase the efficiency of photovoltaic cells, the surface of the photovoltaic cell should be cooled. It is also assumed that as the temperature of the PV panels increases every 10 °C, the degradation rate doubles. A side effect of the sunlight that falls on PV panels is the thermal energy produced in this process, in addition to electricity. The design of photovoltaic thermal (PVT) devices is usually based on classical photovoltaic panels. Moreover, a special cooling module can be installed below the photovoltaic cells to improve their efficiency.

Skoplaki and *Palyvos* in [1,2] studied the external conditions that affect the operation of photovoltaic panels. By cooling the solar cells with a stream of fluid, such as air or water, the electricity yield can be improved. However, a conceptually better design is to reuse the heat energy that the coolant emits [3,4]. In liquid PVT modules, the heat sink is characterized by a lower heat transfer coefficient, lower density, lower heat capacity, and lower thermal conductivity. Water is used most often as a working medium in liquid modules, which is characterized by higher density, increased heat capacity, and thermal conductivity compared to air PVT modules [5]. *Bergene* and *Løvvik* in [6] developed a detailed physical model of the PVT/w flat collector by which the overall efficiency was estimated. *Garg* et al. conducted mathematical and experimental studies of PVT systems [7,8]. *De Vries* investigated the operation of several PVT collector designs. The single-glazed structure has been shown to be superior to the structure without glazing (which has an unfavorable thermal efficiency) or double glazing (which has an unfavorable electrical efficiency). By transient analysis, *Prakash* in [9] pointed out that the air collector design has a lower thermal efficiency than the water collector due to the inferior heat transfer between the thermal absorber and the air stream. *Rockendorf* et al. in [10] compared the performance of a thermoelectric collector (producing heat first, then electricity) and a PVT/w collector (in a sheet-and-tube design). The electric power of the PVT/w collector was found to be significantly higher than that of the thermoelectric collector.

Generally, the reported thermal efficiency of practical PVT/liquid systems is generally in the range of 45 - 70% for unglazed and glazed collector designs. For flat PVT/air systems, the optimum thermal efficiency can reach 55%.

Akbarzadeh and *Wadowski* investigated the design of a new panel cooling based on a heat pipe [11]. The thermosiphon or gravity-assisted heat pipe is a completely passive system that transfers heat from one place to another. The proposed cooling system for the rear part of the solar cells included two interconnected heat exchangers, preempted and filled with R-11, R-22, and water refrigerants. *Bai et al.* in [12] presented a simulation study of the use of PVT/in collectors as water heating devices in a solar-assisted heat pump

* Corresponding author: dstrak@tu.kielce.pl

system. *Hollick* evaluated the improvement of the energy efficiency of a system in which solar cells were attached to a metal trapezoidal sheet on the vertical facades of buildings [13].

In [14], Eulerian two-fluid model coupled with the extended wall boiling model was used to simulate the departure from nucleate boiling (DNB) in vertical heated tubes under high pressure using Simcenter STAR-CCM+. CFD calculations were performed with different wall heat fluxes. A two-fluid model coupled with an extended wall boiling model was used to simulate DNB in vertical heated tubes with both uniform and nonuniform heat fluxes. In [15] in order to obtain data to correlate cross-flow resistance coefficient, a computational fluid dynamic simulation using Star-CCM+ was performed for the flow of water through a 5 × 5 rod bundle geometry supported by a spacer grid with split mixing. The two layer k-epsilon turbulence model was used with an all y+ automatic wall treatment function in Simcenter STAR-CCM+. Correlations were presents to determine the resistance coefficient to cross-flow.

This paper aims to present a new construction of a compact plate heat exchanger dedicated to PVT cooling. The photovoltaic cell constitutes the heated wall of a counter-current heat exchanger with rectangular minichannels. The CAD model of a heat exchanger with minichannels was proposed. CFD calculations were performed using Simcenter STAR-CCM+ software. The fluid temperature and velocity profile in the minichannels were determined. Furthermore, temperature distributions on the heat exchanger's plates – fluids contact surfaces were achieved. Finally, local heat transfer coefficients were obtained.

At Kielce University of Technology, research on flow boiling heat transfer in minichannels has been provided for many years. For the analysis of the experimental data, analytical - numerical methods such as: Trefftz and Piccard methods [16], Trefftz and Beck methods [16,17], in which the calculations were based on the use of Trefftz functions. Furthermore, the commercial ADINA program was applied in numerical calculations to perform advanced mathematical procedures using experimental data [18,19]. Similarly, the results of the CFD and heat transfer calculations for the test section with a group of minichannels performed in Simcenter STAR-CCM + software were presented in [20].

2 Experimental stand and preliminary tests

The schematic diagram of the experimental stand is shown in Fig. 1. The most important circuits realized in the experimental setup are two closed loops of working fluids, including:

i) 'hot' fluid loop, in which the FC-72 fluid circulates,
ii) 'cold' fluid loop, in which distilled water circulation occurs.

Other systems implemented at the setup include: the data and image acquisition system and the power supply and control system.

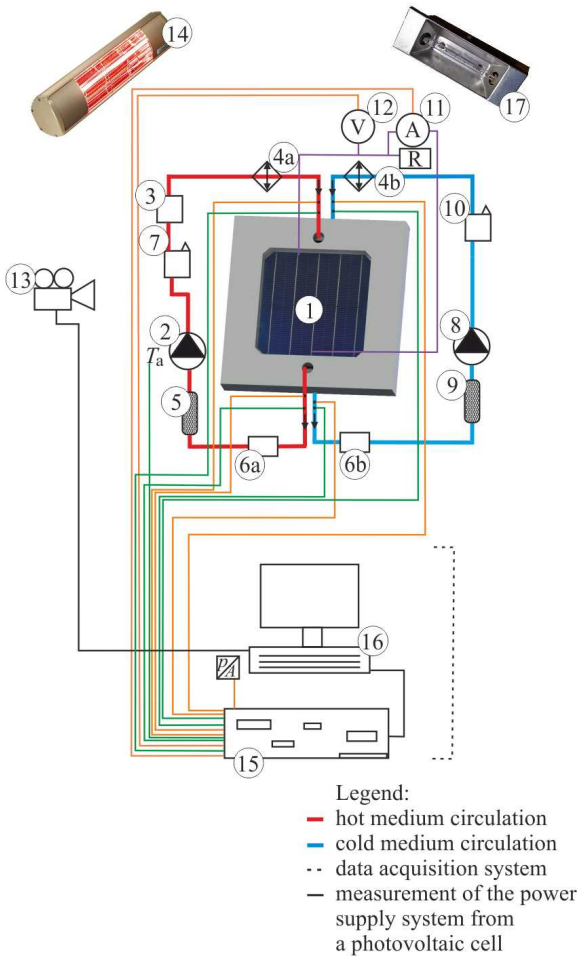

Fig. 1. Schematic diagram of the experimental stand: 1 – test module with minichannels, 2,8 – circulating pumps, 3 – flow regulator, 4 – heat exchanger, 5,9 – filters, 6a, 6b – flow meter, 7,10 – air separators, 11 – ammeter, 12 – voltmeter, 13 – thermal imaging camera, 14 – infrared heater, 15 – data acquisition station, 16 – computer, 17 – halogen lamp, T_a – ambient temperature, p_a – ambient pressure, R – receiver load (a light bulb).

The view of the test module with minichannels for cooling photovoltaic panels is shown in Fig. 2.

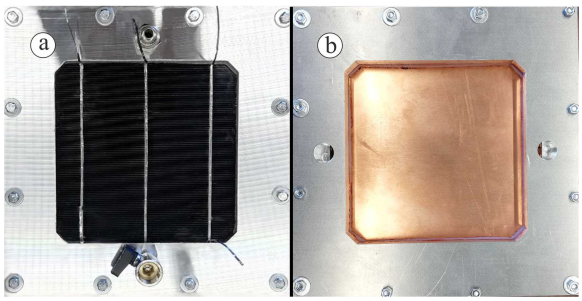

Fig. 2. View of the test module: a) side of the solar panel, b) side of a copper plate.

Figure 2a presents a view of the test module from the side of the PV panel and Fig. 2b shows the back part of the module with a visible copper plate. The PV panel has dimensions of 156 mm in width and 156 mm in length, as well as 4 mm in thickness. A counter-current flow of the working fluids in minichannels is required. The flow of both fluids is laminar.

The individual components of the test module are shown in Fig. 3. Its main elements are two parallel copper plates (2, 4) and the PV cell plate (6). A group of 12 parallel minichannels (six 'hot' minichannels and six 'cold' ones) with a rectangular cross section (each 1.5 mm deep, 20 mm width and 70 mm length) is produced between them.

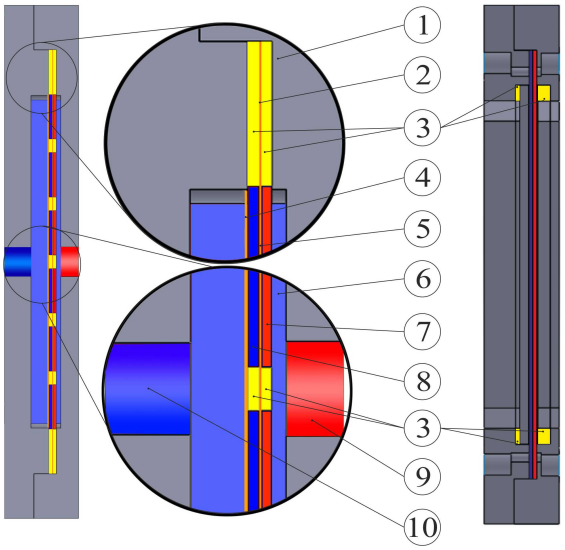

Fig. 3. View of the layers of the PV-T panel cooled with minichannels: 1 – cover (aluminium), 2 – middle plate (copper), 3 – silicone gasket, 4 – outer plate (copper), 6 – PV cell panel, 7 – 'hot' minichanel, 8 – 'cold' minichanel, 9 – inlet/outlet of the 'hot' minichanel, 10 – inlet/outlet of the 'cold' minichanel.

Two selected minichannels of each type are illustrated in Fig. 3 (7, 8). In the minichannels, there is a flow of the FC-72 following fluids: the cooling fluid FC-72 (in the 'hot' minichannels) and distilled water (in the 'cold' minichannels). Additional elements of the test module are four gaskets made of silicon (3).

During experiments, the part of the test module with FC-72 fluid), the outer wall of the minichannel (glass with PV cell) (6), Fig. 3) is heated with an infrared heater (power heating in the range 700 W - 1200 W) and illuminated by a 1000 W halogen bulb.

Heat transfer between the flowing media proceeds through a copper plate (2) with thickness of 0.3 mm. The outer plate of the cold part of the exchanger (4) with thickness of 0.5 mm is also made of copper. The PV panel (6) consists of several thin layers, the first of which is tempered glass (3.2 mm in thickness); the next layer consists of 0.12 mm thick silicon cells, and the lower part contacts the fluid in the minichannel. Type K thermocouples and pressure gauges have been installed at the inlet and outlet of the collectors that supply the minichannels (inlet and outlet collectors). The data from selected experimental series were applied in numerical computations.

3 Simcenter STAR CCM+ numerical calculations

Simcenter STAR-CCM+ software is used for numerical simulation of fluid dynamics based on a wide range of simulation models, including CFD, computational constant mechanics (CSM), electromagnetics, heat transfer, multiphase flow, particle dynamics, reaction flow, electrochemistry, aeroacoustics. It is a simulation tool that provides the most comprehensive set of physical models for computer engineering (CAE) [21].

The numerical computations were provided in the Simcenter Star-CCM+ software. The elements of the 3D model were meshed in version 2020.2.1 Build 15.04.010 (win64/intel18.3vc14-r8 Double Precision).

To perform numerical calculations, a model of the test module with minichannels, intended to cool photovoltaic panels, was assumed in Simcenter STAR-CCM+. The fluid regions consist of the volumes of two fluids: FC-72 and water, for which the flow rates are set, as well as the pressure at the outlet and the fluid temperature at the inlet. In addition, a uniform static temperature on the outer surface of the photovoltaic panel was assumed. A condition of the 'mass flow inlet-type' has been established at the inlets of regions with two liquids, while the 'pressure outlet' has been used as the outlet condition.

Table 1 presents the characteristics of the plates as essential elements of the test module and the experimental data that concern them.

Table 1. Characteristics of the plates and experimental data.

Properties/ Experimental data	Heated plate PV	Copper plate	Closing plate Cu
Thickness, main physical properties			
Thickness, σ [m]	0.004	0.0003	0.0005
Thermal conductivity, λ [W/(m²K)]	1.4	380	380
Density [kg/m³]	2500	8940	8940
Main experimental data			
Temperature, T_{in} [°C]	15	15	15
Temperature, T_{out} [°C]	60	23	18
Static temperature [°C]	50	-	-

Table 2 shows main fluid properties and experimental data. The flow of fluids in the calculations has been described by means of the K-Epsilon model.

Table 2. Main fluid properties and experimental data.

Physical properties/ Experimental data	Fluid FC-72	Distilled water
Main physical properties		
Thermal conductivity, λ [W/(m²K)]	0.06	0.59
Density, [kg/m³]	1713 -1720	999.1 - 992.2
Main experimental data		
Mass flow rate, Q_m [kg/s]	0.0092	0.00556
Temperature, T_{in} [°C]	15	15
Temperature, T_{out} [°C]	29	23
Gauge pressure, p_{in} [bar]	0.1	0.1
Gauge pressure, p_{out} [bar]	0.16	0.61

The geometry of the model heat exchanger with minichannels is presented in Fig. 4.

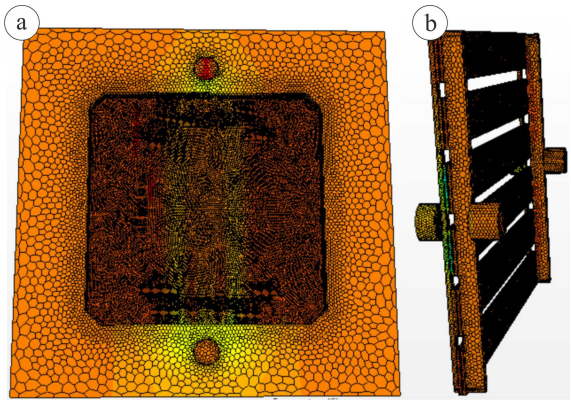

Fig. 4. Model of the test module for numerical calculation in Simcenter STAR-CCM+: a) polyhedral mesh view, b) fluid region flowing in 'hot' minichannel and 'cold' minichannel.

The shape of the exchanger consists of several elements with varying thicknesses. The discretisation of their volume used a polyhedral grid, created based on the tetrahedral grid, using all its advantages in the ability to quickly map the shape of complex geometry. However, by constituting a higher order grid, polyhedral causes the possibility to generate a more accurate result with a smaller number of elements. Additionally, in order to increase the accuracy of the impact of the near-wall layer on the flow profile, the grid was densified around the surfaces of the heated plate, as well as the copper centre plate and the one closing the exchanger. The resulting discretisation effect is shown in Fig. 5.

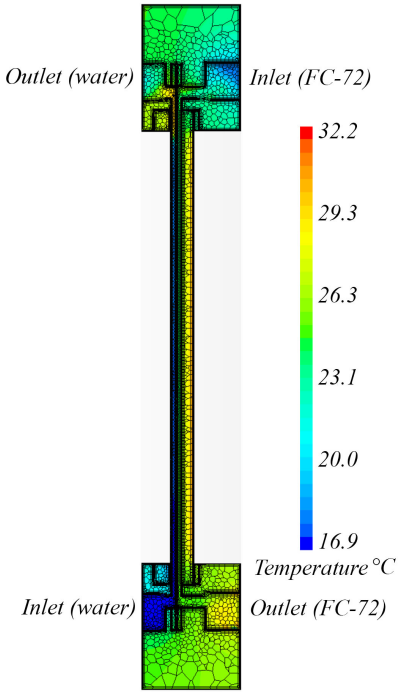

Fig. 5. View of the mesh of the layers of the test module, Simcenter STAR-CCM+.

3.1 CFD calculation results

In Simcenter Star CCM+, computations can be performed in a steady or unsteady condition, taking into account the impact of time on the flow process. In the calculations, a steady state was assumed. For fixed mass flow and inlet pressure values, it was possible to calculate the outlet pressure and the temperature of the fluids. The main objective was to determine the heat transfer coefficient for the individual layers of contact between the fluids and the plates. Multiple iterations of numerical calculations for the same model, with the input mass flow values, enable obtaining the pressure characteristics as a function of flow. Figure 6 presents the residual dependence as a function of iteration. Up to 6500 iterations have been achieved.

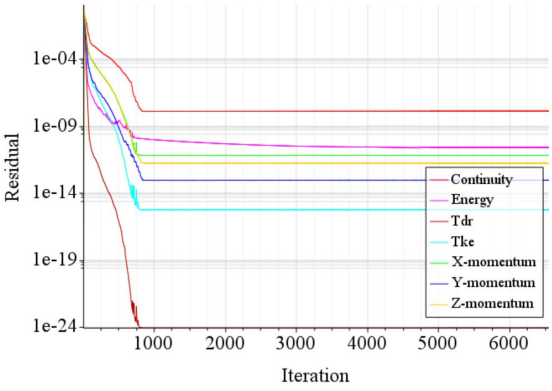

Fig. 6. The residuals as a function of iteration.

The energy was stabilised in the 800th iteration and stayed at 10^{-11}. Continuity stayed at 10^{-8}, for the K-Epsilon model: T_{dr} - the turbulent dissipation rate is at a level of 10^{-24} and T_{ke} - turbulent kinetic energy is at 10^{-16}.

Simcenter Star CCM + software enables visualization of heat and flow parameters. The pressure and flow distributions as the well as temperature distributions in selected cross sections were illustrated as the results of numerical computations, of the basis on the experimental data, shown in Tables 1 and 2. The temperature distribution on the surface of the PV panel/FC-72 flowing in the 'hot' minichannel is given in Fig. 7 and on the contact surface the copper plate/water in the 'cold' minichannel - in Fig. 8.

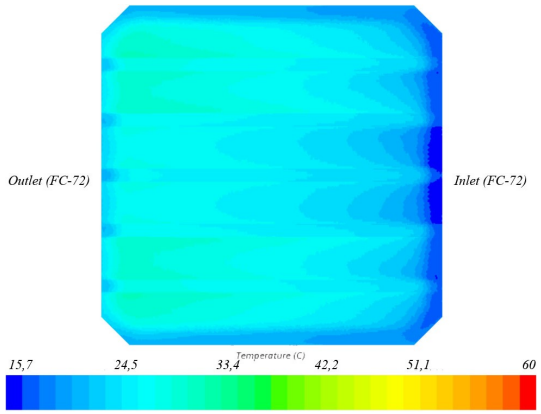

Fig. 7. Temperature on the contact surface: PV panel/FC-72 ('hot' minichannel).

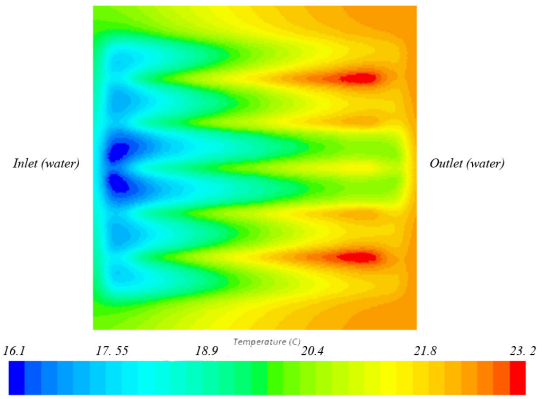

Fig. 8. Temperature on the contact surface: the copper plate/ distilled water ('cold' minichannel).

Analyzing the dependences shown in Figs. 7 and 8, it can be noticed that the temperature increases with the distance from the inlet. The temperature difference on the PV panel/FC-72 contact surface between the inlet and the outlet is approximately 18°C, Fig. 7. It can be underlined that the FC-72 fluid is heated along the flow in minichannels mainly on the contact surface with the PV panel. Compared to the previous difference in temperature, the temperature difference on the contact surface between the copper plate and the distilled water, from the inlet to the outlet, is lower reaching 8°C, Fig. 8.

Calculations of the heat transfer coefficients were performed. The dependence of the heat transfer coefficient as a function of the distance from the minichannel inlet is shown in Fig. 9, for selected fluid layer (cross-section of the minichannel) as follows:

- at the contact surface: the PV panel - FC-72, Fig. 9a, local heat transfer coefficients $\alpha_1(x)$;
- at the contact surface: FC-72 - the copper plate, Fig. 9b, local heat transfer coefficients $\alpha_2(x)$;
- at the contact surface: the copper plate - water, Fig. 9c - local heat transfer coefficients $\alpha_3(x)$.

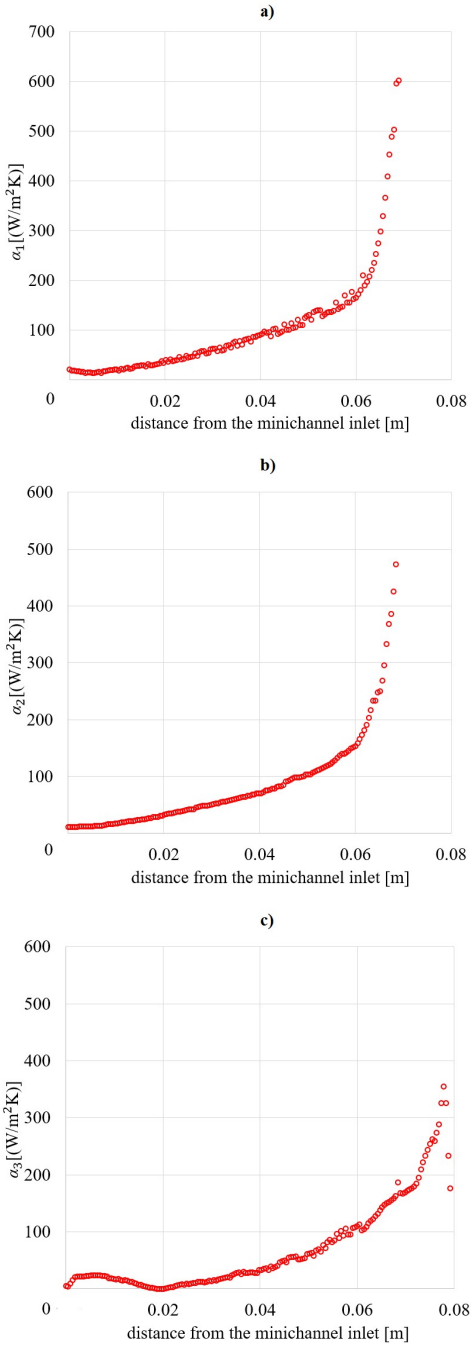

Fig. 9. Heat transfer coefficient versus the distance from the minichannel inlet: a) α_1 - PV panel/FC-72, b) α_2 - FC-72/copper plate, c) α_3 - copper plate/water.

When analyzing dependences showing the heat transfer coefficient versus the distance from the minichannel outlet to inlet, Fig. 9, it is noticed that the heat transfer coefficient decreases with the distance from the minichannel inlet, reaching maximum values near the inlet. Heat transfer coefficient values are in the ranges as follows:

- referring to the contact surface: the photovoltaic panel and FC-72: $\alpha_{1,min}$ = 11 W/(m^{2}K), $\alpha_{1,max}$ = 602 W/(m^2 K),
- referring to the contact surface: FC-72 and the copper plate: $\alpha_{2,min}$ = 8.3 W/(m^{2}K), $\alpha_{2,max}$ = 492.5 W/(m^2 K),
- referring to the contact surface: the copper plate and water: $\alpha_{3,min}$ = 3.7 W/(m^{2}K), $\alpha_{3,max}$ = 346.4 W/(m^2 K).

By comparing both experimental data on the heat transfer coefficient shown in Figs. 9a and 9b, the values of α_2 are lower than those of α_1. As in the case of the heat transfer coefficient α_1, the values of α_2 increase with increasing distance from the channel inlet and the heat flux supplied to the heated plate. When analyzing the data of the heat transfer coefficient presented in Fig. 9c, it can be seen that the coefficient α_3 are lower than α_1 and α_2 values.

The selected dimensionless numbers, mainly Reynolds, Prandtl and Graetz numbers, were determined separately for the minichannel with FC-72 and distilled water. In Table 2 shows the average values of these dimensionless numbers. Reynolds number values indicate laminar flow in both minichannels. Furthermore, the Fanning friction factors for both channels and the overall heat transfer coefficient were calculated and listed in Table 3.

Table 3. Values of selected dimensionless numbers, Fanning friction factors and the overall heat transfer coefficient.

Dimensionless Number	**Average Value**
Reynolds number (FC-72) $\boldsymbol{Re_{FC}}$	1299.3
Reynolds number (water) $\boldsymbol{Re_w}$	577
Prandtl number (FC-72) $\boldsymbol{Pr_{FC}}$	11.7
Prandtl number (water) $\boldsymbol{Pr_{FC}}$	8.1
Graetz number (FC-72) $\boldsymbol{Gz_{FC}}$	185
Graetz number (water) $\boldsymbol{Gz_w}$	55
Fanning friction factor (FC-72) $\boldsymbol{f_{FC}}$	0.018
Fanning friction factor (water) $\boldsymbol{f_w}$	0.047
Overall heat transfer coefficient	**Unit [W/(m^2·K)]**
Overall heat transfer coefficient $\boldsymbol{k}$	523.6

The Reynolds number was calculated as follows:

$$Re = G \cdot d_h / \mu_l \quad (1)$$

where: G - mass flux, d_h - the hydraulic diameter of the minichannel, μ_l – liquid dynamic viscosity.

The following formula was used to calculate the Prandtl number:

$$Pr = \mu_l \cdot c_{p,l} / \lambda_l \quad (2)$$

where: λ_l - liquid thermal conductivity, cp_l - liquid specific heat.

Graetz number was defined according to the formula:

$$Gz = d_h \cdot Re \cdot Pr / L \quad (3)$$

where L - the minichannel length.

When designing heat exchangers, it is important to determine the overall heat transfer coefficient and the Fanning friction factor. For the counter-current heat exchanger, the overall heat transfer coefficient related to the heat transfer area A was calculated as follows:

$$k = Q / A \cdot \Delta T \quad (4)$$

where ΔT means logarithmic mean temperature difference calculated as in [22] and Q is the average of the heat fluxes from the hot and cold minichannels.

The Fanning friction factor f was obtained using the following formula [23,24]:

$$f \cdot Re = 24(1\text{-}1.3553K + 1.9467K^2 - 1.7012K^3 + 0.9564K^4 - 0.2537K^5) \quad (5)$$

where K is the aspect ratio equal to the ratio of the channel width to the depth.

When performing numerical calculations, validation of the results should be taken into account. It should be underlined that the results of the calculations presented in this article were based on experimental data. One of the validation procedures of CFD calculations is to provide a mesh dependence study. This step ensures that the discretization error is known and that it can be quantifiable. In particular, the methodology used is GCI, developed by Roache [25]. Using this methodology, the results of the heat transfer calculation related to the mini-channel heat sink performed in the Simcenter Star-CCM+ software were described in [20]. Furthermore, when comparing the results with those of other authors who applied rectangular minichannels in heat exchanger construction, it can be noticed that the results are similar in the “hot” minichannel as in works [14, 15, 26-32].

In summary, the presented research results should be treated as preliminary. In further research, the analysis of heat transfer in wider thermal and flow parameters, for other working fluids, with a variable spatial orientation of the test module and other dimensions of minichannels.

4 Conclusions

This paper aims to present a new construction of a compact plate heat exchanger dedicated to PVT cooling. The photovoltaic cell constitutes the heated wall of a counter-current heat exchanger with 12 rectangular minichannels. To perform numerical calculations, the CAD model of the test module was created in Simcenter STAR-CCM+ software. Due to the CFD calculations on the data from experiments, the temperature distributions on the heat exchanger plates and fluid contact surfaces were achieved. The temperature distributions indicate that the temperature increases with the distance from the

inlet. Finally, local heat transfer coefficients were determined, presented on graphs, and discussed. It was noticed that the heat transfer coefficient increased with distance from the inlet. Further investigations with a wide range of experimental thermal flow and geometrical parameters, including spatial orientation, are planned.

Acknowledgment

The research reported herein was supported by a grant from the National Science Centre, Poland, No. UMO-2018/31/B/ ST8/01199. The calculations were made using the Simcenter Star-CCM+ software developed by Siemens PLM Software Inc., provided by GMSystem which is a supplier of Siemens Digital Industries Software in Poland.

References

1. E. Skoplaki, J.A. Palyvos, Renew. Energy. **34**, 23–29 (2009)
2 E. Skoplaki, J.A. Palyvos, Sol. Energy. **83**, 614–624 (2009)
3 T.T. Chow, Appl. Energy. **87**, 365–379 (2010).
4 T.T. Chow, G.N. Tiwari, C. Menezo, Int. J. Photoenergy. 307287, 1-17 (2012)
5 M. Souliotis, Y. Tripanagnostopoulos, S.A. Kalogirou, 1-4/2009 **1**, 28–31 (2010).
6 T. Bergene, O.M. Løvvik, Sol. Energy. **55**, 453–462 (1995)
7 H.P. Garg, R.S. Adhikari, Renew. Energy. **11**, 363–385 (1997)
8 H.P. Garg, R.S. Adhikari, Int. J. Energy Res. **23**, 1295–1304 (1999).
9 J. Prakash, Energy Convers. Manag. **35,** 967–972 (1994)
10 G. Rockendorf, R. Sillmann, L. Podlowski, B. Litzenburger, Sol. Energy. **67**, 227–237 (1999).
11 A. Akbarzadeh, T. Wadowski, Appl. Therm. Eng. **16**, 81–87 (1996)
12 Y. Bai, T.T. Chow, C. Ménézo, P. Dupeyrat, Int. J. Photoenergy, 265838 (2012)
13 J.C. Hollick, Renew. energy. **15**, 195–200 (1998).
14 Q. Li, M. Avramova, Y. Jiao, P. Chen, J. Yu, Z. Pu, J. Chen, Nucl. Eng. Des. **326**, 403–412 (2018)
15 V.Y. Agbodemegbe, X. Cheng, E.H.K. Akaho, F.K.A. Allotey, Nucl. Eng. Des. **285**, 134–149 (2015)
16. M. Piasecka, S. Hożejowska, B. Maciejewska, A. Pawińska, Energies, **14**, 1832 (2021)
17. B. Maciejewska, K. Strak, M. Piasecka, Int. J. Numer. Methods Heat Fluid Flow. **28** (2018)
18. M. Piasecka, B. Maciejewska, P. Łabędzki, Energies. **13**, 6647 (2020)
19. B. Maciejewska, P. Łabędzki, A. Piasecki, M. Piasecka, EPJ Web Conf. **143** (2017)
20. M. Piasecka, A. Piasecki, N. Dadas, Energies,**15**, 536 (2022)
21. https://www.plm.automation.siemens.com/global/en /products/simcenter/STAR-CCM.html.
22. J. H. IV Lienhard, J. H. V. Lienhard, 5rd ed. Phlogiston Press Cambridge, MA, USA (2019)
23. W. Rybiński, J. Mikielewicz, Arch. Thermodyn. **35**, 29–42 (2014)
24. R.K. Shah, A.L. J. Fluids Eng. **102** (2) 431–455 (1978)
25. P. J. Roache, J. Fluids Eng. Trans. ASME, 116, **3**, 405–413, (1994)
26. M. Piasecka, S. Hożejowska, A. Pawińska, D. Strąk, Energies, **15**, 1340 (2022)
27. K.R. Anderson,; M. Devost, W. Pakdee, N. Krishnamoorthy, J. Electron. Cool. Therm. Control. **03**, 144–154 (2013)
28. P. Dąbrowski, R. Kumar, Int. Commun. Heat Mass Transf. **129**, 105685 (2021)
29. J. Duan, J. Zhao, X. Li, S. Panchal, J. Yuan, R. Fraser, M. Fowler, Energies, **14**, 4187 (2021)
30. H.A. Zondag, Renew. Sustain. Energy Rev. **12**, 891–959 (2008)
31. M. Fattahi, K. Vaferi, M. Vajdi, F. Sadegh Moghanlou, A. Sabahi Namini, M. Shahedi Asl, Ceram. Int. **46**, 11647–11657 (2020)
32. H. Alizadeh, M. Alhuyi Nazari, R. Ghasempour, M.B Shafii, A. Akbarzadeh, Sol. Energy, **206**, 455–463 (2020)